Volume
2

Micro and Nano Robotics in Medicine

Editor-in-chief | Jaydev P Desai
Edited by | Antoine Ferreira

The Encyclopedia of MEDICAL ROBOTICS

In 4 Volumes

World Scientific

The Encyclopedia of MEDICAL ROBOTICS

Volume 2

Micro and Nano Robotics in Medicine

Editor-in-chief

Jaydev P Desai

Georgia Institute of Technology, USA

Edited by

Antoine Ferreira

Institut National des Sciences Appliquées Centre Val de Loire, campus Bourges, France

World Scientific

CONTENTS

Chapter 6

ELECTROMAGNETIC ACTUATED MICRO- AND NANOROBOTS

Hyunchul Choi, Jong-Oh Park, and Sukho Park

School of Mechanical Engineering, Chonnam National University
Gwangju, Republic of Korea

In this chapter, we present a proposed electromagnetic actuation (EMA) system for micro/nanorobots, which have been widely researched worldwide. First, the intrinsic characteristics of various types of coils used in the proposed EMA system are described. Second, the fundamental theories of the alignment and propulsion of micro/nanorobots using the proposed EMA system in an actuation mechanism are summarized. Third, the configuration and principles of the various types of the proposed EMA system in the 2D and 3D locomotion of the micro/nanorobots are described. Finally, diverse applications, including medical applications of micro/nanorobots using the proposed EMA system are described.

1. Introduction

Medical micro/nanorobots have been studied in recent research.[1–5] Compared with previous surgical procedures, medical micro/nanorobots are non-invasive or minimally invasive because of their small size. In addition, because medical micro/nanorobots accurately deliver therapeutic drugs to target lesions, they might minimize the side effects of overdoses of therapeutic drugs.[6] However, in medical micro/nanorobots, it is difficult to integrate the actuator, power source, and controller in their bodies because of their limited size. To minimize this limitation, external devices are used to realize the main functions of medical micro/nanorobots. In particular, wireless micro/nanorobots could be inserted into human organs, which should provide various steering, locomotive, and therapeutic

functions for the diagnosis and treatment of the diseases. Therefore, external magnetic actuation methods have been widely researched for the locomotion of micro/nanorobots.

Martel *et al.* adopted a magnetic field that was generated by the medical magnetic resonance imaging (MRI) of gradient coils to actuate a microrobot.[7–10] The MRI coils manipulated the paramagnetic microrobot while simultaneously recognizing its position. They also demonstrated the feasibility of drug delivery by using the microrobot in blood vessels. Nelson *et al.* proposed a bacterial flagella-inspired microrobot and an intraocular microrobot, both of which used an external electromagnetic field.[11–13] The bacterial flagella-inspired microrobot had a spiral-shaped body. It was propelled by a rotational magnetic field that was generated by three pairs of orthogonally stationary Helmholtz coils. The intraocular microrobot was actuated by an electromagnetic field that was generated by the OctoMag magnetic manipulation system.[13] The electromagnetic field could be controlled easily and rapidly by changing the current in the coil. Sitti *et al.* demonstrated the stick–slip locomotion of a microrobot using the electromagnetic actuation (EMA) system.[14,15] When the microrobot was placed on a uniform bottom surface, the stick–slip motion of the microrobot was generated and applied to the manipulation of microparticles on a substrate. In a typical application of micromanipulation using an electromagnetic microrobot, they demonstrated a microgripper robot that used a soft magnet, which manipulated the microstructures in 3D space. Arai developed a microrobot using an EMA system that used three pairs of Helmholtz coils.[16,17] The locomotion of the microrobot synchronized with the drilling. The microrobot was rotated about its axis by the rotational magnetic field that was generated by the Helmholtz coil pairs. Because the microrobot had a spiral shape body, its rotation generated a thrusting force and locomotion. When the microrobot reached a blocked vessel, it drilled through the blockage. Swimming robots using electromagnetic fields have also been proposed.[18] The electromagnetic fields were changed by the coil currents, and the swimming robots were controlled through variations in the electromagnetic fields.

In this chapter, first, we present the coil structures used in our proposed EMA system and their intrinsic characteristics. Second, we summarize the basic theories of the alignment and propulsion of the micro/nanorobots using the proposed EMA systems. Third, we describe the configuration and principles of the various types of the proposed EMA systems for 2D and 3D locomotion of the micro/nanorobot. Finally, we introduce diverse applications of the micro/nanorobots using the proposed EMA systems, including medical applications.

2. Coil Structures for an Electromagnetic Actuation (EMA) System

Several basic functions are necessary in order to actuate micro/nanorobots. First, they are aligned in a desired direction. A uniform magnetic field is generated in the desired direction through uniform electromagnetic coils, such as Helmholtz coils and uniform saddle coils. Next, to generate the propulsion force of the micro/nanorobot, a uniform gradient magnetic field along each axis is generated through gradient electromagnetic coils, such as Maxwell coils and gradient saddle coils.

Circular Helmholtz coils (HCs) create a uniform magnetic flux, and Maxwell coils (MCs) generate a uniform gradient magnetic flux.[19,20] These widely used coils have simple structures. Therefore, various EMA systems consisting of HCs and MCs have been proposed. Because of the physical interferences of HC and MC, however, EMA systems that use HC and MC have large volumes and low power efficiency.[35] To overcome these undesirable properties, we propose electromagnetic coils with saddle shapes, which have the same functions as the HC and MC. Similar to HCs, uniform saddle coils (USCs) can generate a uniform magnetic flux in the region of interest (ROI). In addition, similar to MCs, gradient saddle coils (GSCs) can generate a uniform gradient magnetic flux in the ROI.

2.1. *Conventional Helmholtz and Maxwell coils*

Generally, HCs consist of two pairs of solenoids. To generate a uniform magnetic flux, the radius r of the HC solenoid equals the distance between two solenoids.[21,22] The current of the HC flows in the same direction and has the same intensity. One pair of HCs can generate a uniform magnetic flux along the axis. Figure 1 shows a circular HC and a field map in ROI. The magnetic flux produced by a circular type HC is described as follows:

$$\vec{H}_h = \begin{bmatrix} d_h & 0 & 0 \end{bmatrix}^T, \tag{1}$$

$$d_h = 0.7155 \times \frac{i_h \times n_h}{r_h}, \tag{2}$$

where i_h, n_h, and r_h are the current, turns, and radius of the circular HC, respectively.

Similar to circular HCs, square Helmholtz coils (SHC) are used to generate a uniform magnetic field in ROI.[23] Figure 2 shows a square HC and a field map in ROI, where the distance of the square type HCs is determined as 1.0890a (a: half of the side in the square). As shown in Fig. 2, square HCs can also generate a uniform magnetic flux in ROI.

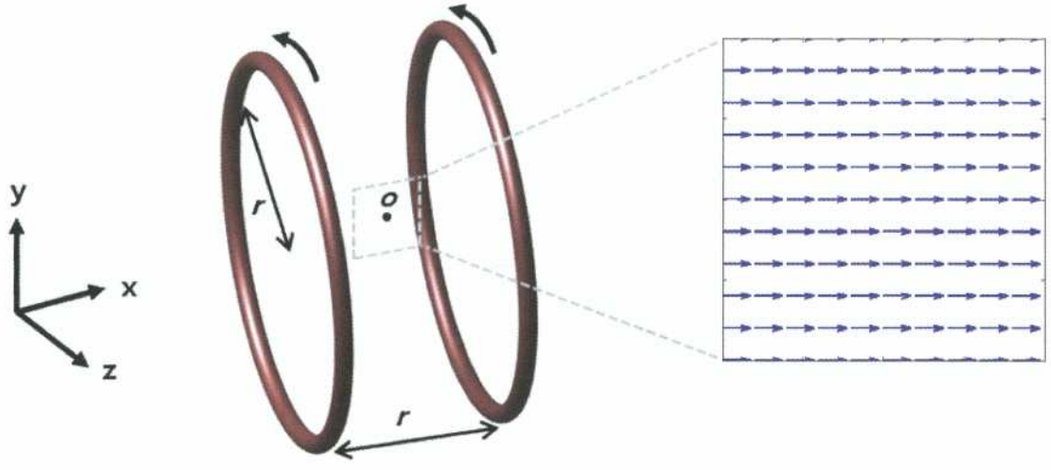

Figure 1. Circular HC and field map in ROI (HC-*fx*), where HC-*fx* is the fixed HCs along the x-axis.

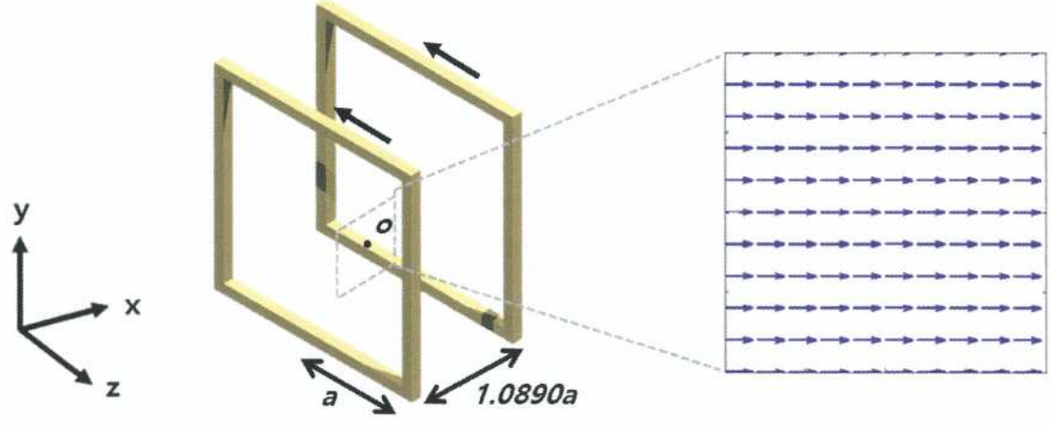

Figure 2. Square HCs and field map in ROI (SHC-*fx*), where SHC-*fx* is the fixed square HC along the x-axis.

Figure 3 shows the configuration of a Mc and the magnetic field map in ROI. Generally, the MC consists of a pair of solenoid coils and has the relation of $=\sqrt{3}r$, where d denotes the distance between the two solenoid coils and r is the radius of the solenoid. The applied current intensities of a MC are the same, but the current flows in the opposite direction. The magnetic field near the center of the MC is expressed as follows:

$$\vec{H}_m = \begin{bmatrix} g_m x & -0.5 g_m y & -0.5 g_m z \end{bmatrix}^T, \tag{3}$$

$$g_m = 0.6413 \times \frac{i_m \times n_m}{r_m^2}, \tag{4}$$

where i_m, n_m, and r_m are the current, turns, and radius of the circular MC, respectively. As shown in Fig. 4 and Eq. (3), we found that the uniform gradient magnetic fluxes were generated along the x-, y-, and z-axes.

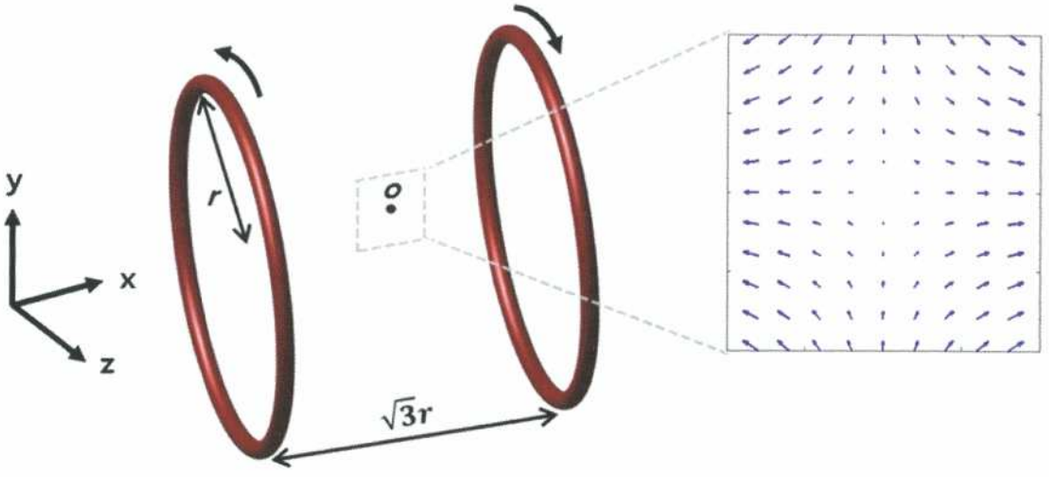

Figure 3. Circular type MC and field map in ROI (MC-*fx*), where MC-*fx* indicates that the fixed MCs are along the x-axis.

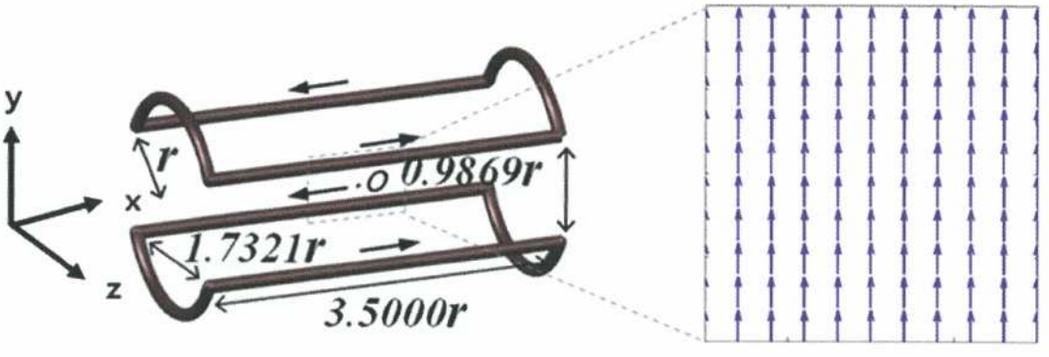

Figure 4. USC and field map in ROI (USC-*fy*), where USC-*fy* is the fixed USCs along the y-axis.

2.2. *Saddle coils*

The saddle type coils with the same functions of HC and MC were proposed.[29,30] Figure 4 shows the schematic diagram of the USC and the magnetic field map in the ROI. As shown in Fig. 4, USC is composed of the straight and arc coils. The generated magnetic field in ROI can be determined by the summation of each coils (the straight and arc coils). Therefore, the magnetic flux produced by the USC is described as follows:

$$\vec{H}_{\text{us}} = [0 \quad d_{\text{us}} \quad 0]^T, \tag{5}$$

$$d_{\text{us}} = 0.6004 \times \frac{i_{\text{us}} \times n_{\text{us}}}{r_{\text{us}}}, \tag{6}$$

where i_{us}, n_{us}, and r_{us} are the current, turns, and radius of the uniform saddle coil, respectively. As shown in Fig. 4 and Eq. (5), we found that the USC (USC-*fy*) could generate a uniform magnetic flux along the y-axis.

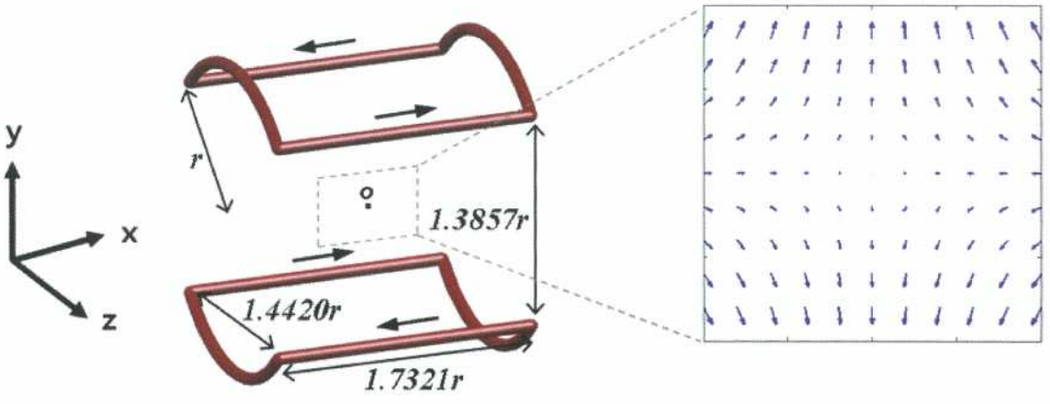

Figure 5. GSC and field map in ROI (GSC-fy), where GSC-fy is the fixed USCs along the y-axis.

Figure 5 shows a schematic diagram of the GSC and the magnetic field map in the ROI. Similar to the USC, the GSC is composed of straight and arched coils. The magnetic field generated in ROI can be determined by the summation of each coil (both straight and arched coils). The magnetic flux produced by the GSC is described as follows:

$$\vec{H}_{\mathrm{gs}} = \begin{bmatrix} g_{\mathrm{gs}}x & -2.4398g_{\mathrm{gs}}y & 1.4398g_{\mathrm{gs}}\mathrm{z} \end{bmatrix}^T, \tag{7}$$

$$g_{\mathrm{gs}} = 0.3286 \times \frac{i_{\mathrm{gs}} \times n_{\mathrm{gs}}}{r_{\mathrm{gs}}^2}, \tag{8}$$

where i_{gs}, n_{gs}, and r_{gs} are the current, turns, and radius of the GSC, respectively. As shown in Fig. 5 and Eq. (7), we found that the uniform gradient magnetic fluxes were generated along the x-, y-, and z-axes.

3. Electromagnet Actuation Mechanism of the Micro/Nanorobot Using Magnetic Rotation Torque and Propulsion Force

In general, both HC and USC can generate a uniform magnetic field. Therefore, when a micro/nanorobot with magnetic materials is located in the ROI, and it is not aligned in the direction of the uniform magnetic field, the following rotation torque is generated[19]:

$$\tau = V\mathbf{M} \times \mathbf{B}, \tag{9}$$

where τ, V, $\mathbf{M}$, and $\mathbf{B}$ are the rotation torque, volume, magnetization of the micro/nanorobot, and external magnetic flux, respectively.

As shown Fig. 6(a), to align the micro/nanorobot in the desired direction, two pairs of uniform coils (HC, USC) are arranged along the x- and y-axes.[24,25] By using two pairs of uniform coils, a uniform magnetic field is generated, and the micro/nanorobot with magnetic materials can be aligned in the desired direction.

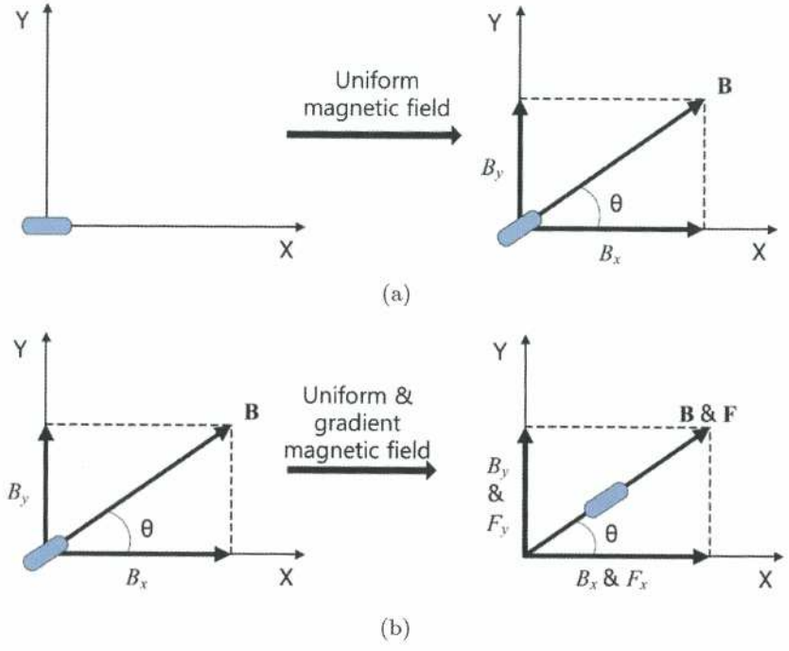

Figure 6. Electromagnet actuation mechanism of the micro/nanorobot. (a) Rotation of the micro/nanorobot by uniform magnetic field. (b) Propulsion of the micro/nanorobot by uniform and gradient magnetic fields.

From Eq. (9), the rotation torque generated by the uniform magnetic field is derived as follows:

$$\tau = V\left(M_x B_y - M_y B_x\right)\mathbf{k}, \tag{10}$$

where M_x and M_y denote the magnetization value of each axis, B_x and B_y are the magnetic fluxes, and $\mathbf{k}$ is the unit vectors of z-axis. Therefore, if a micro/nanorobot with magnetic materials is misaligned with the desired direction (θ), a rotation torque is generated, which rotates the robot in the desired direction. When the micro/nanorobot is aligned in the desired direction, the torque becomes zero, and the magnetization value of each axis is expressed as $M_x = M\cos\theta$ and $M_y = M\sin\theta$.

After the alignment of the magnetic micro/nanorobot, the uniform gradient magnetic field generates a propulsion magnetic force in the desired direction, as shown in Fig. 6(b). The propulsion magnetic force in each direction is described as follows:

$$\begin{bmatrix} F_x \\ F_y \end{bmatrix} = V \begin{bmatrix} M\cos\theta g_x \\ M\sin\theta g_y \end{bmatrix}, \tag{11}$$

where g_x and g_y denote the uniform magnetic field gradient of each axis.

4. EMA Systems for 2D Locomotion

In the previous section, we described the various coils (HC, SHC, MC, USC, and GSC) and the electromagnet actuation mechanism of the micro/nanorobot. In this section, we describe various EMA systems that can be used for the locomotive control of a micro/nanorobot in a 2D plane. The EMA systems for the locomotion of the micro/nanorobot are shown in in Fig. 7.

First, the fundamental EMA system consists of two pairs of Hc and MC[25–27] that are perpendicular to the x- and y-axes. HCs create a uniform magnetic field. The magnetic field generated by each pair of HCs is defined as a magnetic field vector. The vector sum of the magnetic field is considered the final magnetic field along the desired direction in the 2D plane. The magnetic field on the x- and y-axes from each HC is described as follows[25]:

$$\begin{bmatrix} B_x \\ B_y \end{bmatrix} = \begin{bmatrix} B\cos\theta \\ B\sin\theta \end{bmatrix}, \tag{12}$$

where B_x and B_y denote the uniform magnetic field of each axis and B denotes the uniform magnetic field in the desired direction.

The gradient coils are used to generate the propulsion force of the micro/nanorobot in the desired direction.[25–27] Generally, MCs (gradient coils) generate a uniform gradient magnetic field in the axial and perpendicular direction. From Eqs. (3) and (11), the force exerted by the two pairs of MCs on the magnetic propulsion of the magnetic micro/nanorobot on the $x-y$ plane is described as follows:

$$\begin{bmatrix} F_x \\ F_y \end{bmatrix} = V \begin{bmatrix} M\cos\theta(g_{m,x} - 0.5g_{m,y}) \\ M\sin\theta(g_{m,y} - 0.5g_{m,x}) \end{bmatrix}. \tag{13}$$

When $g_{m,x} = g_{m,y}$ is satisfied, the magnetic propulsion force of the magnetic micro/nanorobot is generated in the aligned direction.

Second, similar to the EMA system with two pairs of Hc and MC, two pairs of HCs are perpendicularly arranged along the x- and y-axes, and one pair of MCs is positioned along the z-axis.[28] Because of the reduction to one pair of MCs, the EMA system with two pairs of HCs and one pair of MCs has a smaller volume and lower power consumption compared with the EMA system with two pairs of HCs and MCs.

Third, the EMA system for 2D locomotion is developed, which is composed of one pair of HC and MC and one pair of USC and GSC.[29,30] HC and USC are used for the alignment of the magnetic micro/nanorobot in the desired direction. The magnetic field on the x- and y-axes from each coil is described in Eq. (12). The

Number [Ref.]	Coil structure	Diagram	Coil system	Movement
2D-1 [25-27]	HC-fx HC-fy MC-fx MC-fy	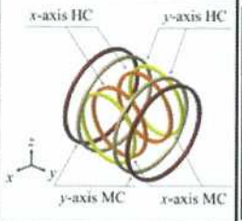	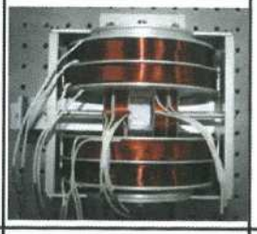	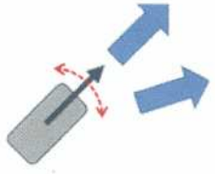
2D-2 [28]	HC-fx HC-fy MC-fz	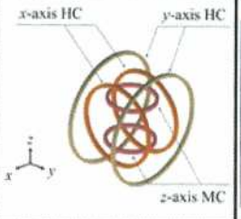	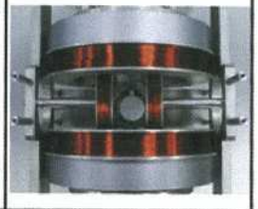	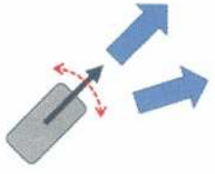
2D-3 [29-30]	HC-fx USC-fy MC-fx GSC-fy	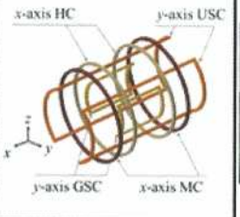	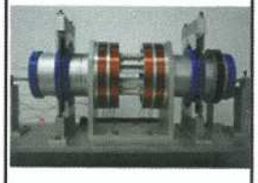	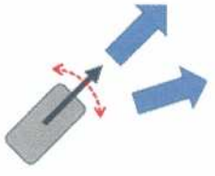
2D-4 [31]	Coil-fx Coil'-fx Coil-fy Coil'-fy	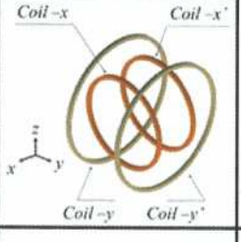		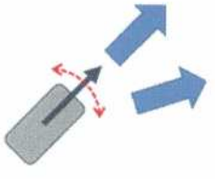
2D-5 [32]	HC-fx HC-fy HC-fz MC-fx	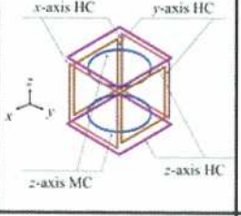		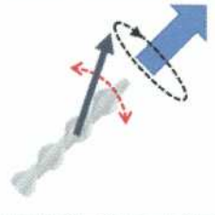
2D-6 [33]	HC-fx USC-fy USC-fz MC-fx GSC-fy	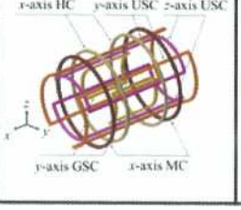	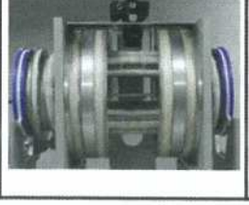	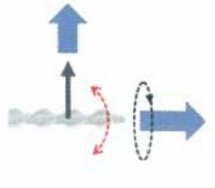

Figure 7. EMA systems for 2D locomotion.

magnetic propulsion force generated by the MC and GSC is expressed as follows:

$$\begin{bmatrix} F_x \\ F_y \end{bmatrix} = V \begin{bmatrix} M\cos\theta(g_{gs} + g_m) \\ M\sin\theta(-2.4398g_{gs} - 0.5g_m) \end{bmatrix}. \tag{14}$$

In order that the magnetic propulsion force of the magnetic micro/nanorobot is generated in the aligned direction, the following relationship should be satisfied:

$$g_m = -2.2932g_{gs}. \tag{15}$$

The previously mentioned EMA systems use individual coils for the alignment and propulsion of the micro/nanorobot. That is, the uniform coils (HC and USC) are used for the alignment, and the gradient coils (MC and GSC) are used for the propulsion of the micro/nanorobot. Therefore, the EMA systems have large volumes and high power consumption.

Fourth, in order to solve the disadvantages of the previous EMA systems, we propose a new EMA system, which has only two pairs of stationary circular coils.[31] Through the control of the magnitude and direction of the current applied to each coil in the EMA system, the micro/nanorobot is aligned and propelled in the desired direction. In addition, through the position recognition of the micro/nanorobot by using a CCD camera, the precise position control of the micro/nanorobot is possible.

Fifth, we proposed a spiral-type microrobot, which is actuated by a rotational external magnetic field. The spiral-type microrobot generated a thrusting force and showed a locomotive ability in the 2D plane.[32] For the control of the spiral microrobot, the EMA system consists of three pairs of HCs along the x-, y-, and z-axes, respectively, where the thrusting force of the microrobot mainly depends on the spiral shape, the viscosity of the fluid, and the rotating frequency. However, the thrusting force is too small and very weak. To overcome this problem, the thrusting force of the microrobot is enhanced by using a pair of MCs (MC-*fz*).

Finally, we proposed an EMA system with three pairs of uniform coils (HC-*fx*, USC-*fy*, and USC-*fz*) and two pairs of gradient coils (MC-*fx*, GSC-*fy*).[33] This EMA system shows not only the rotational motion but also the translational motion of the spiral-type microrobot.

Based on the EMA systems proposed for the 2D locomotion of the micro/nanorobots shown in Fig. 7, we demonstrated various locomotion tests, which are shown in Fig. 8. Figure 8(a) shows fundamental directional propulsion tests of the microrobot and the tests conducted to track the desired paths. Figure 8(b) shows the manipulation of microbeads by the microrobot using the EMA system. Figure 8(c) shows the directional errors of the microrobot caused by a distortion in the magnetic field in the EMA system. It also shows the compensation using a feedforward and feedback algorithm, in which the precise position control of the microrobot is possible through a feedback control using a CCD camera.

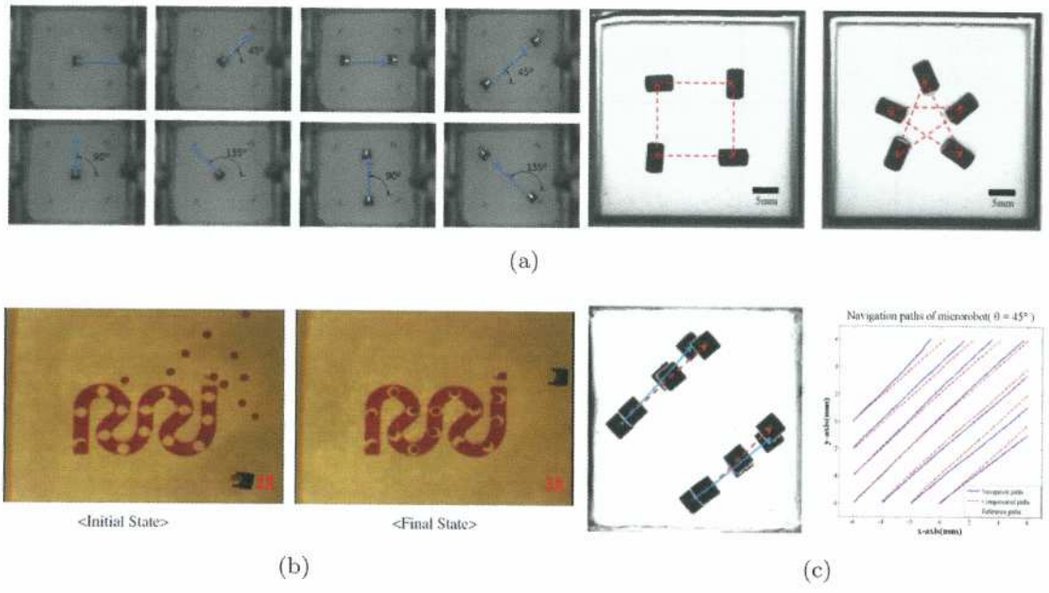

Figure 8. EMA systems for 2D locomotion. (a) Rotation and propulsion of microrobot by HC and MC. (b) Manipulation test of non-magnetic particles using EMA system. (c) Position-based compensation test of EMA system.

5. EMA Systems for 3D Locomotion

In this section, we describe the various EMA systems used to control the micro/nanorobot in 3D space. Figure 9 provides a summary of the EMA systems used for the 3D locomotion of the micro/nanorobots. The EMA systems for 3D locomotion can be divided into the following two types. First, the previous EMA system used for 2D locomotion was expanded to 3D actuation by adding a rotational axis.[34–37] That is, the 2D working space in the previous EMA system was expanded to a 3D working space for 3D locomotion through the rotation of the 2D working space (i.e. $x-r$ working plane). This is particularly appropriate when the micro/nanorobot moves within a 3D tubular space, such as blood vessels and digestive tracts (i.e. small and large intestine). As shown in Fig. 9, the EMA systems have an $x-r$ working plane and a rotational motion of r-axis coils on the x-axis. Second, we proposed EMA systems used for the 3D locomotion of the microrobots, which consist of three pairs of stationary HCs and one pair of stationary MCs along the z-axis.[38,39] In particular, a pair of rotating MC on z-axis was added to the EMA system.[38] The two EMA systems were actuated by similar operational method and both have an $r-z$ working plane for the 3D locomotion of the microrobots.

Next, we describe the detailed structures of the EMA systems for 3D locomotion. First, for the simple coil structure of the EMA system used for the 3D locomotion shown in Fig. 10, we used one pair of stationary HC–MC on the x-axis (HC-*fx*, MC-*fx*) and one pair of rotational HC–MC on the x-axis (HC-*rx*, MC-*rx*)

Number [Ref.]	Coil structure	Diagram	Coil system	Movement
3D-1 [34]	HC-fx MC-fx HC-rx MC-rx	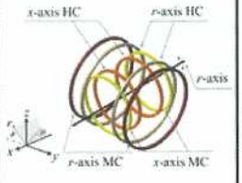		• x-r plane 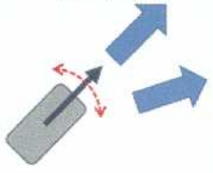
3D-2 [35]	HC-fx MC-fx USC-rx GSC-rx	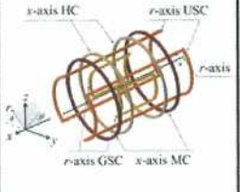	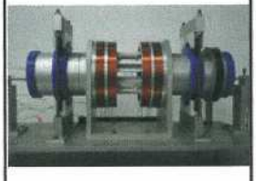	• x-r plane 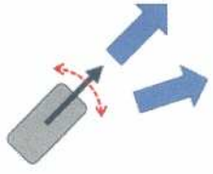
3D-3 [36]	HC-fx USC-rx GSC-r'x	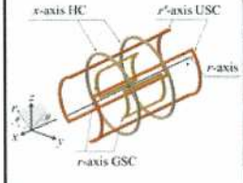		• x-r plane 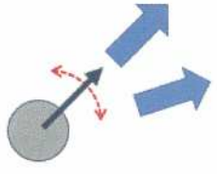
3D-4 [37]	Coil-fx Coil'-fx Coil-ry Coil'-ry	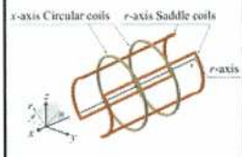	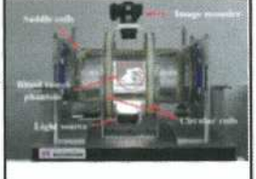	• x-r plane 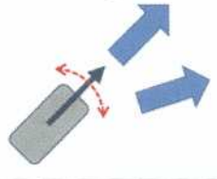
3D-5 [38]	HC-fx HC-fy HC-fz MC-fz MC-rz	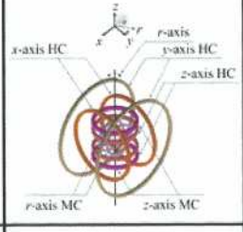		• r-z plane 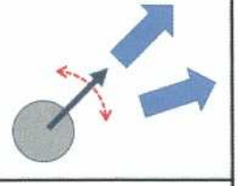
3D-6 [39]	HC-fx HC-fy HC-fz MC-fz	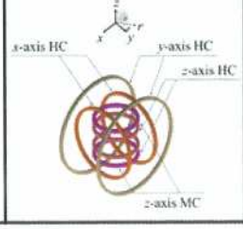		• r-z plane 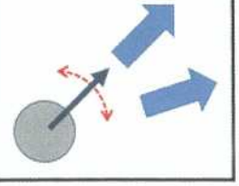

Figure 9. EMA systems for 3D locomotion. f (fix), r (rotation).

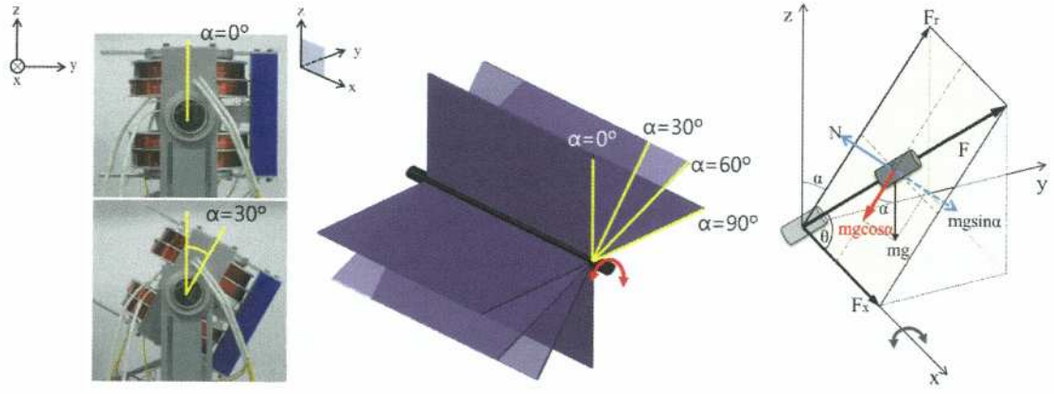

Figure 10. EMA systems for 3D locomotion.

to achieve the 3D locomotion of the micro/nanorobot.[34] The simple EMA system is expanded to the 3D EMA system (3D-1 in Fig. 9) by using two pairs of stationary HC–MC (2D-1 in Fig. 7) on the x- and y-axes (HC-*fx*, MC-*fx*, HC-*fy*, and MC-*fy*) through the rotation of the 2D working plane.

As shown in Fig. 10, by using the rotational coil pairs, the actuation mechanism of the 2D locomotion EMA system can be expanded to the 3D locomotion of the microrobot. Figure 10 shows the rotational coil pairs and the corresponding actuation plane of the EMA system. Based on the rotational angle (α), the gravitational force can be divided into a normal component ($\text{mg}\sin\alpha$) and a tangential component ($\text{mg}\cos\alpha$). The reaction force cancels the normal component, but the tangential component remains. Therefore, the tangential component of the gravitational force required compensation. We compensated the tangential component of the gravitational force by using the following equation:

$$\frac{F_r - \text{mg}\cos\alpha}{F_x} = \tan\theta, \tag{16}$$

where F_x, F_r, mg, α, and θ are the x-axis magnetic force, r-axis magnetic force, gravitational force, rotational angle of the $x-r$ plane, and magnetization direction of the micro/nanorobot in $x-r$ plane, respectively.

Second, the 3D EMA system (3D-2 in Fig. 9) was developed based on the EMA system (2D-2 in Fig. 7). The 3D EMA system uses one pair of stationary HC–MC on the x-axis (HC-*fx*, MC-*fx*) and one pair rotational USC–GCS on the x-axis (USC-*rx*, GSC-*rx*) to achieve the 3D locomotion of the micro/nanorobot.[35] The actuation mechanism of the EMA system is similar to the previous 3D locomotive mechanism of the 3D EMA system (3D-1).

Third, the EMA system (3D-3) consists of one pair of stationary HCs on the x-axis (HC-*fx*) and one pair of rotational USC-GSC on the x-axis (USC-*rx*, GSC-$r'x$) to achieve 3D locomotion of the micro/nanorobot.[36] The comparison of

the two 3D EMA systems (3D-2 and 3D-3 in Fig. 9) showed that the 3D-3 EMA system does not have a fixed MC as in the 3D-2 EMA system. However, it is able to create motions that are similar to those achieved by the 3D-2 EMA system. The alignment of the microrobot is controlled by the HC on the x-axis and the USC on the x-axis (aligned in the r-axis). The magnetic propulsion force is generated by the GSC on the x-axis (aligned with the r'-axis).

Fourth, the 3D-4 EMA system consists of four coils (two stationary circular coils and two rotational saddle coils), which are the same as the pair of stationary HCs on the x-axis (coil-fx, coil′-fx), and one pair of rotational uniform saddle coils on the x-axis (coil-rx, coil′-rx).[37] Because the current intensity and directions of the four coils are individually controlled, the alignment and propulsion of the microrobot are achieved.

Fifth, the 3D-5 EMA system consists of three pairs of stationary HCs, one pair of stationary MCs on the z-axis, and one pair of rotating MCs on the z-axis.[38] The three pairs of stationary HCs are used for the alignment and rotation of the micro/nanorobot, and the stationary MC on the z-axis and the rotational MC on the z-axis are used for the propulsive magnetic force of the micro/nanorobot in 3D space.

Finally, the coil structure of the 3D-6 EMA system is similar to that of the 3D-5 EMA system. However, it only has a stationary MC on the z-axis. It does not have a rotational MC because the gradient magnetic field occurs on the x-, y-, and z-axes, as derived from Eq. (3).[39] Therefore, the microrobot is aligned by the uniform magnetic field with three pairs of HCs. The propulsion of the microrobot is controlled by the gradient magnetic field on the r- and z-axes by positioning a MC on the z-axis. Because the 3D-6 EMA system does not have a rotating coil, the r-axis was created, and the microrobot is controlled in the plane consisting of the r-axis and the z-axis in 3D locomotion.

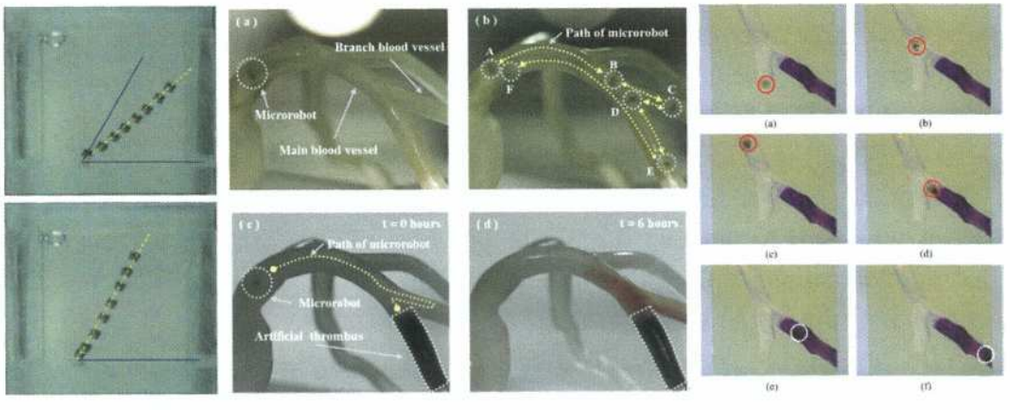

Figure 11. EMA systems for 3D locomotion.

Figure 11 shows 3D locomotion of the microrobot using the proposed 3D EMA systems. Through the 3D locomotion, the microrobot traveled to a target lesion and performed therapeutic motions, such as therapeutic drug delivery and drilling an occlusion. We, therefore, demonstrated the potential of microrobots using the 3D EMA system in medical applications, such as specific drug delivery and clot removal.

6. Applications

Sections 4 and 5 described various EMA systems used for the 2D and 3D locomotion of the micro/nanorobot. In this section, we introduce several applications that use the proposed EMA systems, such as a swimming robot, a blood vessel therapeutic microrobot, a spiral-type microrobot, a microrobot that manipulates microparticles, and an active locomotive capsule endoscope.

6.1. *Swimming robots*

Many organs in the human body, such as blood vessels and ventricles, are filled with fluid. For efficient actuation in a fluid environment, bioinspired swimming robots, such as the fish, tadpole, and jellyfish, have been proposed. In particular, we proposed a tadpole-inspired swimming microrobot with a simple structure and easy control mechanism.[40,41] Because the tadpole microrobot was precisely controlled using three pairs of HCs, we demonstrated various swimming motions in a fluid.

In addition, a jellyfish-like swimming microrobot was proposed,[42] which consists of a main body with four fins (PDMS), four NdFeB magnets, and a buoyant head in the center of the body. In addition, the jellyfish-like swimming microrobot is controlled using three pairs of rectangular HCs. We demonstrated various 3D swimming motions of this microrobot (Fig. 12).

Number [Reference]	Coil structure	Coil system	Microrobot	Movement
Swimming Tadpole microrobot [40-41]	HC-fx HC-fy HC-fz		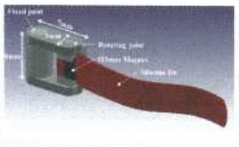	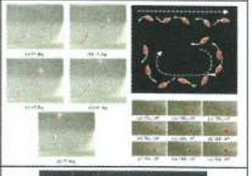
Jellyfish robot [42]	HC-fx HC-fy HC-fz		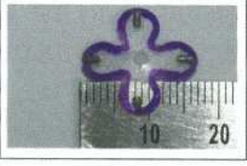	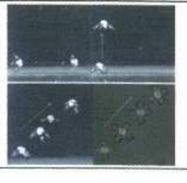

Figure 12. Swimming microrobots: a swimming tadpole microrobot and a jellyfish robot.

Number [Reference]	Coil structure	Coil system	Microrobot	Movement
ITMS [44-45]	HC-fx MC-fx USC-rx GSC-rx			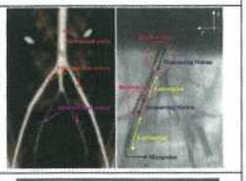
Spiral type microrobot [32-33]	HC-fx HC-fy HC-fz MC-fz		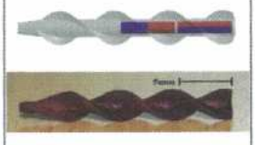	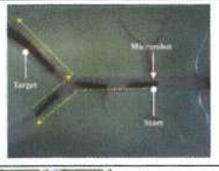
Sphere type microrobot with bur [36,38-39]	HC-fx HC-fy HC-fz MC-fz MC-rz		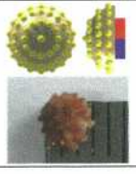	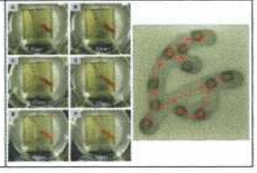

Figure 13. Intravascular therapeutic microrobot system.

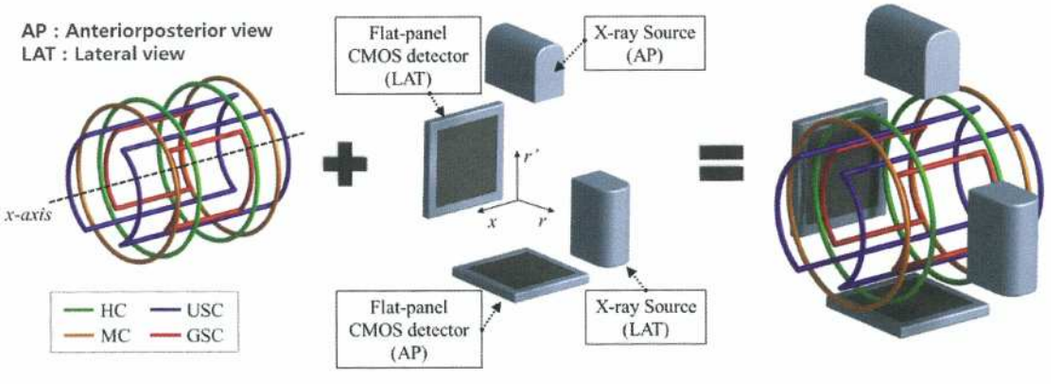

Figure 14. Intravascular therapeutic microrobot system with bi-plane X-ray.

6.2. *Intravascular therapeutic microrobots*

Previous research anticipated that microrobot technologies would be applied in intravascular therapy. First, much research has been conducted on the use of intravascular therapeutic microrobots, and several examples of this robotic system have been proposed.[43–45] In the intravascular therapeutic microrobot system (ITMS), the coil structure must be applied easily in a human body (Fig. 13). Therefore, among the previous proposed coil structures used in EMA systems, a combination of saddle coils could be a good candidate. In addition, the microrobot should have 3D locomotion in 3D blood vessels. Therefore, we designed the coil structure for an ITMS, which consists of one pair of stationary HC–MC on the x-axis and one pair of rotational USC–GSC on the x-axis, as shown in Fig. 14.

In addition, the position of the microrobot should be recognized in its locomotion of in 3D blood vessels. Therefore, we adopted a bi-plane X-ray imaging device for an ITMS, which generates images of the anterior–posterior (AP) view and the lateral view (LAT). Figure 14 shows the arrangement of the coils and the bi-plane X-ray imaging device. As shown in Fig. 14, the bi-plane X-ray imaging device is rotated with one pair of rotational USC–GSC on the x-axis. That is, the x-ray source and detector always must be located on the r- and r'-axes.

By using the proposed EMA system and the bi-plane X-ray device, we demonstrated the locomotion of the microrobot from the abdominal artery to the iliac artery in a blood vessel in the pulsatile flow of a live pig.[44,45] Based on the two X-ray images, we estimated the exact position of the microrobot in the blood vessel of the animal's body. Consequently, the proposed therapeutic microrobot showed that it was a feasible intravascular therapeutic medical device. Hence, it will be developed for use in the treatment of vascular diseases.

Second, we expected that a microrobot could be used for the mechanical penetration of a clot in a blood vessel. Therefore, we proposed a spiral-type microrobot, which is rotated by a rotational external magnetic field.[32,33] Using a 3D printer, we fabricated a spiral-shaped microrobot and inserted a small permanent magnet into its body. The spiral-type microrobot showed locomotion to and penetration of the clot in a phantom blood vessel by using the rotational magnetic field of the EMA system, as shown in Fig. 13.

Finally, a sphere-type microrobot with burrs on its surface was proposed for use in vascular therapy.[36,38,39] SiO_2 powder was used to fabricate the roughly burred surface of this microrobot. In addition, similar to the spiral-type microrobot, the sphere-type microrobot showed locomotion to the phantom blood vessel where if drilled a clot using the rotational magnetic field of the EMA system, as shown in Fig. 13.

6.3. *Microparticle manipulation microrobot*

Magnetically actuated microrobots were proposed to manipulate micro particles (cell, protein, and bead).[27,46,47] First, the shape and size of the microrobot should be appropriate for the manipulation of micro particles. Using the 2D EMA system shown in Fig. 15, the magnetically actuated microrobot was aligned and propelled in the desired direction along the $x-y$ plane, and it successfully manipulated the micro particles. We demonstrated that the microrobot could deliver the microparticles to their target positions. Through the repeated manipulation of the microparticles, the microparticles were arranged into various patterns, as shown in Fig. 15.

Number [Reference]	Coil structure	Coil system	Microrobot	Movement
Micro-particles manipulation microrobot [27]	HC-fx HC-fy MC-fx MC-fy	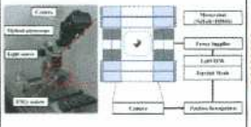		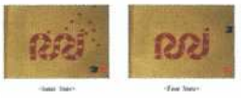

Figure 15. Manipulation of microparticles using a magnetically actuated microrobot.

Number [Reference]	Coil structure	Coil system	Microrobot	Movement
ALICE [50-51]	HC-fx MC-fx USC-rx USC-r'x GSC-rx	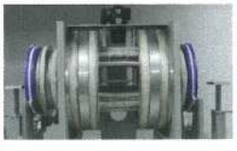		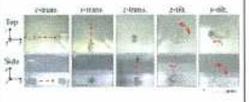

Figure 16. Active locomotive intestinal capsule endoscope.

6.4. *Active locomotive intestinal capsule endoscope (ALICE)*

One of the most active areas of research on the medical uses of EMA systems is the active capsule endoscope.[48–51] Because of the limitations of the conventional flexible endoscopes used in gastrointestinal diagnostic procedures, a wireless capsule endoscope was developed and commercialized. Despite the many advantages of the wireless capsule endoscope, its restricted mobility has limited its use to the diagnosis of the esophagus and small intestine. In particular, it is impossible for a physician to be involved in the diagnostic procedure or to perform active checkups using the conventional capsule endoscope.[50] In addition, much time is required to review the enormous amount of stacked images from the capsule endoscope and to confirm a lesion that is shown in the acquired images.

To solve this problem, we proposed an active locomotive intestinal capsule endoscope (ALICE), which is shown in Fig. 16. Through the active locomotion of ALICE, we expected that the physician could control the device and effectively diagnose diseases of the digestive organs. In addition, the locomotive function of ALICE extends the diagnostic range of the active capsule endoscope to other digestive organs that have a large volume and many folding structures, such as the stomach and colon.

Regarding locomotion, ALICE was aligned and propelled in a desired direction. As shown in Figs. 16 and 17(a), the EMA system aligned and propelled the

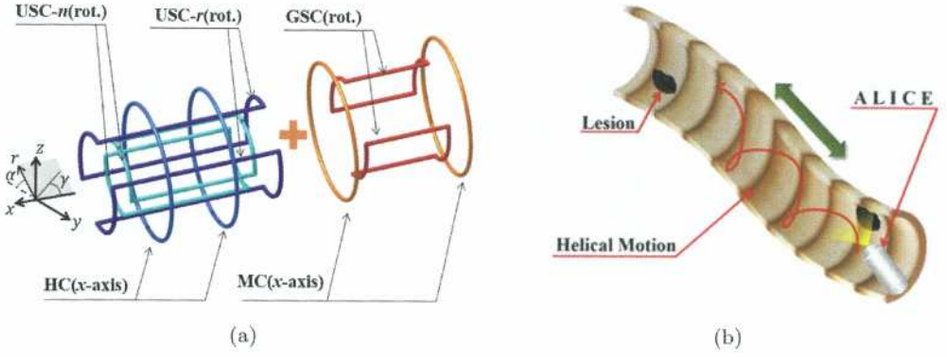

Figure 17. Active locomotive intestinal capsule endoscope. (a) EMA system and (b) helical motion of the ALICE.

capsule endoscope to the desired 3D coordinates via the HC on the x-axis (HC-fx) and two rotating pairs of USCs on the x-axis (USC-rx, USC-$r'x$), which were orthogonally positioned.[50] In addition, as shown in Fig. 17(b), the helical motion (rotational + translational) of the ALICE was made possible by using the proposed EMA system.

In addition, if additional functions were developed and integrated into the capsule endoscope, such as biopsy and drug delivery, it would be a powerful theranostic tool for treatment of the digestive organs. We developed a robotic biopsy device for ALICE, which has a sharp blade that is connected to a shape-memory alloy actuator. To execute the biopsy procedure, the sharp blade is activated and exposed through the supply of a small current to heat the shape-memory alloy actuator. A specific rotational motion of ALICE was generated using the EMA system to extract the tissue sample from the intestines.[51] We demonstrated the feasibility of integrating the shape memory alloy-based biopsy device into ALICE by using the EMA system.

6.5. *A hybrid actuated microrobot using an electromagnetic field and flagellated bacteria*

We expected that the EMA system could be utilized for effective drug delivery when magnetic nanoparticles (MNPs) were included in the drug microbeads. To target the microbeads using the EMA system, the blood vessels are visualized and utilized to control the precise position. However, because of the limitation of the visualization of the small blood vessels, the control of the position of the microbeads was very difficult. Subsequently, a bacteria-based microrobot (the so-called bacteriobot) with a tumor targeting and therapeutic bacteria function was proposed for solid tumor therapy.[52–54] The bacteriobot is a microrobot that consists of a microstructure in which therapeutic bacteria navigate to the tumor. The

Number [Reference]	Coil structure	Coil system	Microrobot	Movement
Hybrid Actuated microrobot [55]	HC-fx HC-fy MC-fx MC-fy	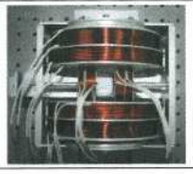		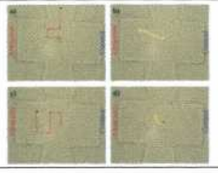

Figure 18. A hybrid actuated microrobot using an electromagnetic field and flagellated bacteria.

microstructure serves as a drug capsule. We expected that the bacteriobot would target a tumor lesion owing to the targeting characteristics of the therapeutic bacteria and could show a therapeutic function for the tumor owing to the therapeutic drug and the therapeutic bacteria. However, we estimated that the bacteriobot would have very small propulsive force and low tumor targeting performance. To overcome the two disadvantages in targeting the microbeads using the EMA system and the bacteriobot, we proposed a hybrid actuated microrobot combined with the EMA and the bacterial actuation.[55] We demonstrated that the hybrid microrobot could be actuated by the electromagnetic field of the EMA system and by the bacterial actuation, as shown in Fig. 18. We expected that the hybrid microrobot would be actuated in the macro-vascular system by the EMA system and propelled by the actuation of the therapeutic bacteria.

7. Conclusions

In this chapter, we explained various coil structures used in EMA systems, and we summarized various EMA systems used for the 2D and 3D locomotion of micro/nanorobots. The precise locomotion of the micro/nanorobot and the particle manipulations were possible through using the 2D EMA systems. The 3D EMA systems could be used for the precise 3D locomotion of the micro/nanorobot in fluids. We concluded that the various EMA systems have the potential to be used in medical applications, such as intravascular therapeutic microrobots, active capsule endoscopy, and specific drug delivery systems.

References

1. Nelson, B., Kaliakatsos, I. and Abbott, J. (2010). Microrobots for minimally invasive medicine. *Ann. Rev. Biomed. Eng.*, 12, 55–85.
2. Abbott, J., Nagy, Z., Beyeler, F. and Nelson, B. (2007). Robotics in the small part I: Microrobotics. *IEEE Robot. Autom. Magaz.*, 14(2), 92–103.
3. Sitti, M., Ceylan, H., Hu, W., Giltinan, J., Turan, M., Yim, S. and Diller, E. (2015). Biomedical applications of untethered mobile milli/microrobots *Proc. IEEE*, 103(2), 205–224.

4. Wang, H. and Pumera, M. (2015). Fabrication of micro/nanoscale motors. *Chem. Rev.*, 115(16), 8704–8735.
5. Brand, O. Fedder, G. K. Hierold, C. Korvink, J. G. and Tabata, O. (2015). In Sun, Y. and Liu, X. (Eds.), *Micro and Nanomanipulation Tools* (John Wiley & Sons).
6. Yan, X., Zhou, Q., Yu, J., Xu, T., Deng, Y., Tang, T., Feng, Q., Bian, L., Zhang, Y., Ferreira, A. and Zhang, L. (2015). Magnetite nanostructured porous hollow helical microswimmers for targeted delivery. *Adv. Funct. Mater.*, 25(33), 5333–5342.
7. Martel, S., Felfoul, O., Mathieu, J. B., Chanu, A., Tamaz, S., Mohammadi, M., Mankiewicz, M. and Tabatabaei, N. (2009). MRI-based medical nanorobotic platform for the control of magnetic nanoparticles and flagellated bacteria for target interventions in human capillaries. *The Int. J. Robot. Res.*, 28(9), 1169–1182.
8. Pouponneau, P., Leroux, J. C., Soulez, G., Gaboury, L. and Martel, S. (2011). Co-encapsulation of magnetic nanoparticles and doxorubicin into biodegradable microcarriers for deep tissue targeting by vascular MRI navigation. *Biomaterials*, 32(13), 3481–3486.
9. Pierre, P., Bringout, G. and Martel, S. (2014). MR Imaging of Therapeutic magnetic microcarriers guided by magnetic resonance navigation for enhanced liver chemoembolization: A design review. *Ann. Biomed. Eng.*, 42(5), 929–939.
10. Martel, S. (2013). Magnetic navigation control of micro agents in the vascular network: Challenges and strategies for endovascular magnetic navigation control of microscale drug delivery carriers. *IEEE Control Syst.*, 33(6), 119–134.
11. Zhang, L., Peyer, K. E. and Nelson, B. J. (2010). Artificial bacterial flagella for micromanipulation. *Lab on a Chip*, 10(17), 2203–2215.
12. Mahoney, A. W., Nelson, N. D., Peyer, K. E., Nelson, B. J. and Abbott, J. J. (2014). Behavior of rotating magnetic microrobots above the step-out frequency with application to control of multi-microrobot systems. *Appl. Phys. Lett.*, 104(14), 144101.
13. Kummer, M. P., Abbott, J. J., Kratochvil, B. E., Borer, R., Sengul, A. and Nelson, B. J. (2010). OctoMag: An electromagnetic system for 5-DOF wireless micromanipulation. *IEEE Trans. Robot.*, 26(6), 1006–1017.
14. Pawashe, C., Floyd, S. and Sitti, M. (2009). Multiple magnetic microrobot control using electrostatic anchoring. *Appl. Phys. Lett.*, 94(16), 164108.
15. Diller, E. and Sitti, M. (2014). Three-dimensional programmable assembly by untethered magnetic robotic micro-grippers. *Adv. Funct. Mater.*, 24(28), 4397–4404.
16. Ishiyama, K., Sendoh, M. and Arai, K. I. (2002). Magnetic micromachines for medical applications. *J. Magnet. Magnet. Mater.* 242–245(1), 41–46.
17. Sendoh, M., Yamazaki, A., Chiba, A., Soma, M., Ishiyama, K. and Arai, K. I. (2004). Spiral type magnetic micro actuators for medical applications. In *Micro-Nanomechatronics and Human Science, and the Fourth Symposium Micro-Nanomechatronics for Information-Based Society*, pp. 319–324.
18. Chu, W., Lee, K., Song, S., Han, M., Lee, J., Kim, H., Kim, M., Park, Y., Cho, K. and Ahn, S. (2012). Review of biomimetic underwater robots using smart actuators. *Int. J. Precis. Eng. Manufact.*, 13(7), 1281–1292.
19. Hayt, W. H. and Buck, J. A. (2006). *Engineering Electromagnetic*, (McGraw-Hill, New York).
20. Cacak, R. K. and Craig, J. R. (1969). Magnetic field uniformity around near-Helmholtz coil configurations. *Rev. Sci. Instrum.*, 40(11), 1468–1470.
21. Yesin, K. B., Vollmers, K. and Nelson, B. J. (2006). Modeling and control of untethered biomicrorobots in a fluidic environment using electromagnetic fields. *Int. J. Robot. Res.* 25(5–6), 527–536.
22. Han, B., Park, S. and Lee, Y. (2008). Gradient waveform synthesis for magnetic propulsion using MRI gradient coils. *Phys. Med. Biol.*, 53(17), 4639.

23. Alamgir, A. K. M., Fang, J., Gu, C. and Han, Z. (2005). Square Helmholtz coil with homogeneous field for magnetic measurement of longer HTS tapes. *Physica C: Superconductivity*, 424(1), 17–24.
24. Lucarini, G., Palagi, S., Beccai, L. and Menciassi, A. (2014). A power-efficient propulsion method for magnetic microrobots. *Int. J. Adv. Robot. Syst.*, 11(1), 116.
25. Choi, H., Choi, J., Jang, G., Park, J. and Park, S. (2009). Two-dimensional actuation of a microrobot with a stationary two-pair coil system. *Smart Mater. Struct.*, 18(5), 1–9.
26. Choi, J., Choi, H., Jeong, S., Park, B., Ko, S., Park, J. and Park, S. (2013). Position-based compensation of electromagnetic fields interference for electromagnetic locomotive microrobot. In *Proc. Institut. Mech. Eng., Part C: J. Mech. Eng. Sci.*, 227(9), 1915–1926.
27. Go, G., Kwak, D., Piao, L., Choi, H., Jeong, S., Lee, C., Park, B., Ko, S., Park, J. and Park, S. (2013). Manipulation of micro-particles using a magnetically actuated microrobot. *Mechatronics*, 23(18), 1037–1043.
28. Choi, H., Choi, J., Jeong, S., Yu, C., Park, J. and Park, S. (2009). Two-dimensional locomotion of a microrobot with a novel stationary electromagnetic actuation system. *Smart Mater. Struct.*, 18(11), 1–6.
29. Jeon, S., Jang, G., Choi, H. and Park, S. (2010). Magnetic navigation system with gradient and uniform saddle coils for the wireless manipulation of micro-robots in human blood vessels. *IEEE Trans. Magnet.*, 46(6), 1943–1946.
30. Jeon, S., Jang, G., Choi, H., Park, S. and Park, J. (2011). Utilization of magnetic gradients in a magnetic navigation system for the translational motion of a micro-robot in human blood vessels. *IEEE Trans. Magnet.*, 47(10), 2403–2406.
31. Go, G., Choi, H., Jeong, S., Lee, C., Park, B., Ko, S., Park, J. and Park, S. (2014). Position-based magnetic field control for an electromagnetic actuated microrobot system. *Sensors Actuators A: Phys.*, 205(1), 215–223.
32. Jeong, S., Choi, H., Cha, K., Li, J., Park, J. and Park, S. (2011). Enhanced locomotive and drilling microrobot using precessional and gradient magnetic field. *Sensors Actuators A: Phys.*, 171(2), 429–435.
33. Jeon, S., Jang, G., Choi, H., Park, S. and Park, J. (2012). Magnetic navigation system for the precise helical and translational motions of a microrobot in human blood vessels. *J. Appl. Phys.*, 11(7), 07E702.
34. Jeong, S., Choi, H., Choi, J., Yu, C., Park, J. and Park, S. (2010). Novel electromagnetic actuation (EMA) method for 3-Dimensional locomotion of intravascular microrobot. *Sensors Actuators A: Phys.*, 157(1), 118–125.
35. Choi, H., Cha, K., Choi, J., Jeong, S., Jeon, S., Jang, G., Park, J. and Park, S. (2010). EMA system with gradient and uniform saddle coils for 3-D locomotion of microrobot. *Sensors Actuators A: Phys.*, 163(1), 410–417.
36. Choi, H., Jeong, S., Lee, C., Go, G., Ko, S., Park, J. and Park, S. (2015). Simplified electromagnetic actuation system for three dimensional locomotive and drilling microrobot. *Proc. Institu. Mech. Eng.: Part C*, 229(13), 2443–2454.
37. Go, G., Choi, H., Jeong, S., Lee, C., Ko, S., Park, J. and Park, S. (2015). Electromagnetic navigation system using simple coil structure (4 Coils) for 3D locomotive microrobot. *IEEE Trans. Magnet.*, 51(4), 8002107.
38. Yu, C., Kim, J., Choi, H., Choi, J., Jeong, S., Cha, K., Park, J. and Park, S. (2010). Novel electromagnetic actuation system for three-dimensional locomotion and drilling of intravascular microrobot. *Sensors Actuators A: Phys.*, 161(1), 297–304.
39. Choi, H., Cha, K., Jeong, S., Park, J. and Park, S. (2013). 3-D locomotive and drilling microrobot using novel stationary EMA system. *IEEE Trans. Mechatron.* 18(3), 1221–1225.
40. Byun, D., Choi, J., Cha, K., Park, J. and Park, S. (2011). Swimming microrobot actuated by two pairs of Helmholtz coil system. *Mechatronics*, 21(1), 357–364.

41. Choi, H., Jeong, S., Lee, C., Park, B., Ko, S., Park, J. and Park, S. (2014). Three-dimensional swimming tadpole mini-robot using three-axis Helmholtz coils. *Int. J. Control, Autom. Syst.*, 12(3), 662–669.
42. Ko, Y., Na, S., Lee, Y., Cha, K., Park, J. and Park, S. (2012). Jellyfish-like swimming microrobot actuated by electromagnetic actuation system. *Smart Mater. Struct.*, 21, 057001.
43. Laurent, A., Fruchard, M. and Ferreira, A. (2012). Endovascular magnetically guided robots: navigation modeling and optimization. *IEEE Trans. Biomed. Eng.*, 59(4), 977–987.
44. Jeong, S., Choi, H., Lee, C., Go, G., Sim, D., Lim, K., Jeong, M., Ko, S., Park, J. and Park, S. (2015). Therapeutic intravascular microrobot through compensation of resistance and mutual inductance in electromagnetic actuation system. *Int. J. Control, Autom. Syst.*, 13(6), 1–11.
45. Jeong, S., Choi, H., Lee, C., Kwon, K., Go, G., Sim, D., Lim, K., Jeong, M., Ko, S., Park, J. and Park, S. (2013). A study on 3D locomotion of intravascular therapeutic microrobot using EMA system, In *International Conference on Control, Automation and Systems*, Gwangju, Korea.
46. Tung, H. W., Sargent, D. F. and Nelson, B. J. (2014). Protein crystal harvesting using the RodBot: a wireless mobile microrobot. *J. Appl. Crystallograp.*, 47(2), 692–700.
47. Tasoglu, S., Diller, E., Guven, S., Sitti, M. and Demirci, U. (2014). Untethered micro-robotic coding of three-dimensional material composition. *Nat. Commun.*, 5.
48. Li, Z., Liao, Z. and McAlindon, M. (2014). *Handbook of Capsule Endoscopy*, (Springer).
49. Simi, M., Gerboni, G., Menciassi, A. and Valdastri, P. (2013). Magnetic torsion spring mechanism for a wireless biopsy capsule. *J. Med. Dev.*, 7(4), 041009.
50. Lee, C., Choi, H., Go, G., Jeong, S., Ko, S., Park, J. and Park, S. (2015). Active locomotive intestinal capsule endoscope (ALICE) system: A prospective feasibility study. *IEEE Trans. Mechatron.*, 20(5), 2067–2074.
51. Le, V. H., Hernando, L. R. Lee, C., Choi, H., Jin, Z., Go, T. N. G., Ko, S., Park, J. and Park, S. (2015). Shape Memory Alloy (SMA) Based Biopsy Device for Active Locomotive Intestinal Capsule Endoscope (ALICE). *Proc. Institut. Mech. Eng., Part H*, 229(3), 255–263.
52. Park, S. J., Park, S. H., Cho, S., Kim, D. M., Lee, Y., Ko, S., Hong, Y., Choy, H. E., Min, J. J., Park, J. and Park, S. (2013). New paradigm for tumor theranostic methodology using bacteria-based microrobot. *Scientific Reports*, 3.
53. Park, D., Park, S. J., Cho, S., Lee, Y., Lee, Y., Min, J., Park, B., Ko, S., Park, J. and Park, S. (2014). Motility analysis of bacteria-based microrobot (bacteriobot) using chemical gradient microchamber. *Biotechnol. Bioeng.*, 111(1), 134–143.
54. Behkam, B. and Sitti, M. (2006). Towards hybrid swimming microrobots: Bacteria assisted propulsion of polystyrene beads. *28th Ann. Int. Conf. IEEE (EMBS '06)*, pp. 2421–2424.
55. Li, D., Choi, H., Cho, S., Jeong, S., Jin, Z., Lee, C., Ko, S., Park, J. and Park, S. (2015). A hybrid actuated microrobot using an electromagnetic field and flagellated bacteria for tumor-targeting therapy. *Biotechnol. Bioeng.*, 112(8), 1623–1631.